Application of Material Nonlinearity to a Composite Pressure Vessel Design

David Cohen*
Hercules Aerospace Company, Magna, Utah 84044

The application of matrix-dominated material nonlinearity to composite structural analysis has been addressed extensively in the literature. Little attention has been given to composite nonlinearity resulting from the fiber strain hardening material nonlinearity when subjected to tensile loads. As the fiber strain-to-failure increases, this effect becomes more important. The main objective of the current investigation was to assess the applicability and improve accuracy resulting from the inclusion of both lamina fiber and resin-dominated material nonlinearities in predictions of composite pressure vessels response to internal pressure loading. Comparison between analytical calculations and measured strain response on pressurized composite vessels shows agreement; however, linear and nonlinear analyses show only small differences. A closer look at the contribution of each of the lamina nonlinear components indicates that the linear analysis produces an average result between the stiffening effect of the fiber and the softening effect of the lamina matrix-dominated material nonlinearities. Further, assessment of the results indicates that the lamina fiber-dominated nonlinearity together with the lamina in-plane shear nonlinearity plays the most significant role in accurate prediction of vessel response. The importance of the lamina transverse nonlinearity (E_{22}) is less clear because this nonlinearity is greatly dependent on the type of damage model incorporated in the analysis.

Nomenclature

E	=	lamina Young's modulus
F	=	curvature of the quadratic nonlinear stress-strain relationship
G	=	lamina shear modulus
n	=	parameter that defines the shape of the nonlinear stress-strain Richard-Blacklock relationship
V_f	=	lamina fiber volume fraction
W	=	strain energy function
ν	=	Poisson's ratio
σ	=	stress
σ^o	=	plastic stress in the Richard-Blacklock nonlinear stress-strain relationship
ϵ	=	strain
ϵ^o	=	σ^o/E^o in the Richard-Blacklock nonlinear stress-strain relationship

Subscripts

A, H	=	pressure vessel's axial and/or hoop strains
f, m	=	fiber and/or matrix moduli
s, t	=	secant and/or tangent moduli
1, 2	=	stress and/or strain at points 1 and 2 on the stress-strain curve
11, 22, 33	=	lamina principal directions along (11), transverse (22), and perpendicular (33) to the fiber
12, 13, 23	=	lamina shear moduli and/or Poisson's ratios in the 1-2, 1-3, and 2-3 planes

Superscript

o	=	initial tangent modulus

Received Feb. 11, 1990; presented as Paper 90-1002 at the 31st AIAA/ASME/ASCE/AHS/ACS Structures, Structural Dynamics, and Materials Conference, Long Beach, CA, April 2-4, 1990; revision received Aug. 6, 1990; accepted for publication Aug. 20, 1990.

*Research Engineer, Components Analysis, Product Engineering, P.O. Box 98. Senior Member AIAA.

Introduction

THE application of matrix-dominated material nonlinearity to composite structural analysis has been addressed extensively in the literature.[1-6] This type of material nonlinearity is associated primarily with the large elastic (or plastic) nonlinear response of a lamina when subjected to in-plane shear loads and, to a lesser extent, transverse loads. Cracks will form as the lamina in a multilayer laminate is subjected to transverse stress that exceeds its in situ strength in this direction. These cracks will lead to a substantial reduction in the stiffness of the lamina in the transverse direction.

Numerous analytical approaches are discussed in the literature that address the type of material nonlinearity previously discussed. For example, the elastic in-plane shear nonlinearity was addressed by a higher-order polynomial expansion of the complementary (or strain) energy to produce higher order terms in the stress-strain relationship.[1] Other examples include the Ramberg-Osgood nonlinear stress-strain relationship[2] and a semiempirical approach in which a piecewise cubic spline interpolation function is used in an incremental constitutive law.[3]

Elastic material nonlinearity in the lamina transverse direction can be addressed in much the same way; however, much more complex issues are involved in the nonlinearity associated with the formation of transverse cracks. Approaches discussed in the literature include the application of fracture mechanics in conjunction with continuum constitutive behavior to model damage accumulation and stiffness reduction[4]; application of a negative tangent modulus following damage initiation, which eventually leads to zero stiffness with increasing load[5]; and the discount method where stiffness in the lamina transverse direction is assumed to be zero following damage initiation.[6]

Little attention has been given to composite nonlinearity resulting from the fiber material nonlinear behavior when subjected to tension loads. As fiber strain-to-failure increases, this effect becomes more important, particularly in structures such as filament wound pressure vessels, where laminate response is fiber dominated. The accurate calculation of strain responses in such structures is critical in burst strength predictions. This is particularly true for space-rated structures, where weight is an important design factor.

The phenomenon of elastic nonlinear stress-strain response of high-strength, high-modulus graphite fiber is well docu-

mented.[7-12] In the bulk of these investigations, this phenomenon is attributed to the changes in the preferred orientation of the graphite layers. These layers form long wrinkled ribbons along the fiber axis. As the fiber is strained in the axial direction, these wrinkles are stretched and their orientation changes, leading to strain hardening of the fiber. Graphite fibers with high strain to failure, such as Hercules AS4 and IM7, show up to a 15% increase in the secant modulus between the initial value and the value at which the fiber fails.

The nonlinear stress-strain response of graphite fiber has been measured by a number of investigators.[10-12] The approach followed in this investigation, which also seems to work well for the Hercules AS4 and IM7 fibers, was proposed by Kowalski.[11] In his empirical model, the fiber material nonlinearity is represented by a second-order Hooke's law $\sigma = E^o\epsilon + F\epsilon^2$ (which is consistent with a third-order polynomial expansion of the strain energy function). The E^o and F elastic coefficients are determined by a least-squares fit of the quadratic model to the tensile tow test data of Hercules IM7 and AS4 fibers.

The lamina nonlinear in-plane shear and transverse tension moduli are characterized by the Richard-Blacklock stress-strain relationship.[13] Data from IM7/55A and AS4/55A 4-in. tubes loaded in torsion and transverse tension to failure are used in the evaluation of the unknown coefficients in this relationship, using nonlinear least-squares regression analysis.

Both the fiber and matrix-dominated nonlinearity are then employed in the analysis of a 36-in. filament wound internally pressurized composite vessel. The main objective of the current investigation was to assess the applicability and improvement in accuracy resulting from the inclusion of the aforementioned material nonlinearities in predictions of composite pressure vessel response to internal pressure loading.

Approach

The fiber and resin material nonlinearity constitutive relations are discussed in the following sections. Two separate nonlinear relations are employed in this investigation. The fiber strain hardening nonlinear response is modeled with a quadratic relation. This relation was chosen because it is particularly useful in the empirical characterization of tow tensile data. The resin-dominated nonlinearity (i.e., the lamina in-plane shear G_{12} and transverse tension E_{22}) are modeled with the Richard-Blacklock relationship.[13] This relationship is helpful in modeling the large nonlinear elastic in-plane shear deformation and the large degradation in E_{22} caused by microdamage using an elastic-plastic relationship.

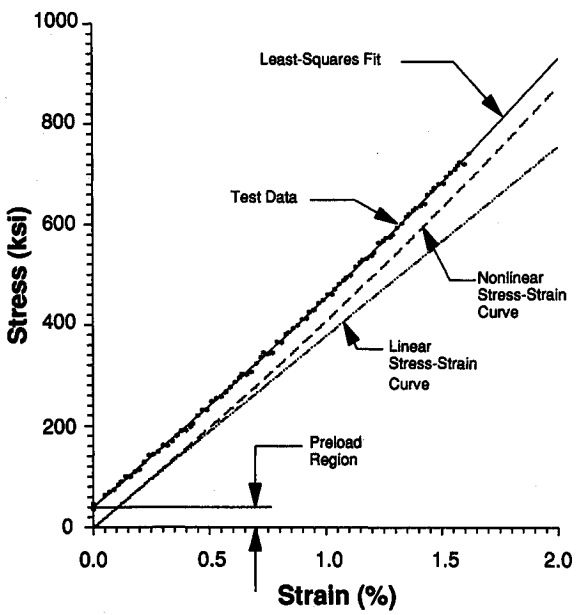

Fig. 1 Tow tensile fiber nonlinear stress-strain response for IM7/55A.

Fiber Nonlinear Constitutive Relation

An empirical quadratic relation[11] was used to model the fiber nonlinear stress-strain characteristics:

$$\sigma(\epsilon) = E^o\epsilon + F\epsilon^2 \tag{1}$$

This relationship is consistent with a third-order polynomial expansion of the strain energy function $W(\epsilon_{ij})$.[1,12] If such a function exists, then the stress-strain relations are derived from

$$\sigma_{ij} = \frac{\partial W}{\partial \epsilon_{ij}} \tag{2}$$

In Eq. (1), E^o can be identified as the initial tangent modulus and F as the curvature of the stress-strain curve that measures the degree of nonlinearity in the fiber. The two elastic coefficients, E^o and F, are determined by a least-squares fit to tow tensile stress-strain data, as shown in Fig. 1. Because such curves generally do not start at zero load (due to a small applied preload to the tow, Fig. 1), empirical curve fitting is accomplished using a generalized quadratic relation:

$$\sigma(\epsilon) = A + B\epsilon + C\epsilon^2 \tag{3}$$

To obtain a stress-strain curve in the form of Eq. (1), which initiates at the origin and is representative of the original test stress-strain curve, the two elastic constants must satisfy the following relations:

$$E^o = \sqrt{B^2 - 4AC}$$

$$F = C$$

This is apparent from the fact that the least-squares fit curve and the nonlinear stress-strain curve are parallel to each other in Fig. 1. Having evaluated E^o and F, the fiber tangent and secant moduli at any point along the stress-strain curve can be determined. The tangent modulus is given by

$$E_t(\epsilon) = \frac{d\sigma}{d\epsilon} = E^o + 2F\epsilon \tag{4}$$

The secant modulus between any two strains ($\epsilon_2 > \epsilon_1$) can be determined by

$$E_s(\epsilon) = \frac{\sigma_2 - \sigma_1}{\epsilon_2 - \epsilon_1} = E^o + F(\epsilon_1 + \epsilon_2) \tag{5}$$

Generally, in a tow test, the modulus is evaluated based on the fiber cross-sectional area, and the resin contribution is neglected. The error resulting from such an assumption is less than 1% for a high-modulus fiber. The lamina modulus (E_{11}) in the fiber direction can then be calculated using the rule-of-mixture and the fiber tangent and/or secant modulus:

$$E_{11} = V_f E_f + (1 - V_f)E_m \tag{6}$$

where E_f is the fiber secant or tangent modulus and E_m is the resin modulus.

The fiber strain hardening nonlinear response could also be easily characterized by the Richard-Blacklock nonlinear stress-strain relationship (to be discussed next). This could have been accomplished by evaluating the parameters in this relationship on the shifted curve derived from the tow tensile data. This was not done in the current investigation; however, for a general methodology development of nonlinear analysis, it may be advisable.

Resin-Dominated Material Nonlinearity

The lamina resin-dominated nonlinear stress-strain behavior is modeled using the Richard-Blacklock[13] relationship:

$$\sigma(\epsilon) = \frac{E^o \epsilon}{\left[1 + \left|\frac{E^o \epsilon}{\sigma^o}\right|^n\right]^{\frac{1}{n}}} \tag{7}$$

where E^o is the lamina initial modulus (E^o_{22} or G^o_{12}), σ^o is the plastic stress, and n is a parameter that defines the shape of the nonlinear stress-strain relationship. An alternative form of this relationship can be obtained by substituting $\epsilon^o = \sigma^o/E^o$ into Eq. (7), such that

$$\sigma(\epsilon) = \frac{E^o \epsilon}{\left[1 + \left|\frac{\epsilon}{\epsilon^o}\right|^n\right]^{\frac{1}{n}}} \tag{8}$$

In Eqs. (7) and (8), the coefficients E^o, σ^o, ϵ^o, and n are determined empirically from 4-in. hoop-wound composite tubular specimens that are loaded in both transverse tension and torsion. The plastic stress (σ^o) is defined as the point at which damage is initiated in the lamina transverse direction. This damage consists primarily of transverse cracks that tend to soften[4,14-16] the lamina stiffness (E_{22}) and, to a lesser degree, the in-plane stiffness (G_{12}).[14] It should be noted that the in situ transverse strength of a transversely constrained lamina can be five times as high as the transverse strength of an unconstrained 90 deg lamina.[16] This in situ strength will depend on the 90 deg ply thickness and the fiber orientation of the constraining plies on either side. By definition, the tangent modulus is given by

$$E_t(\epsilon) = \frac{\partial \sigma}{\partial \epsilon} = \frac{E^o}{\left[1 + \left|\frac{\epsilon}{\epsilon^o}\right|^n\right]^{n+\frac{1}{n}}} \tag{9}$$

The secant modulus is given by

$$E_s(\epsilon) = \frac{\sigma_2 - \sigma_1}{\epsilon_2 - \epsilon_1} = \frac{E^o}{\left[1 + \left|\frac{\epsilon}{\epsilon^o}\right|^n\right]^{\frac{1}{n}}} \tag{10}$$

Composite Pressure Vessel Nonlinear Analysis

The material nonlinearity constitutive relationships discussed above were implemented into a generalized-plane-deformation elasticity solution for multilayer anisotropic cylinders subjected to axisymmetric loads.[17] This type of solution assumes that the cylinder is of infinite length and that the loads do not vary along the vessel's axial direcion. Under this type of analysis, the vessel end, which may be constrained by the test fixtures or the domes, are not accounted for. However, the analysis performed was assumed to be an accurate representation of the state of strain at the midcylinder section away from the ends. The elasticity solution and analysis procedure for multilayer composite cylinders that are subjected to internal pressure and end loads are discussed in detail in Ref. 17.

The only modification to the analysis implemented here was to allow for an iterative solution scheme by which the moduli E_{11}, E_{22}, and G_{12} in each layer are adjusted according to the state of strain in the fiber, transverse, and in-plane shear directions until convergence is satisfied. Because the level of strain in each layer is different, the corresponding values of E_{11}, E_{22}, and G_{12} will also change according to the state of strain in each layer. During the analysis, the lamina E_{11}, E_{22}, and G_{12} moduli are taken as the secant moduli [using Eqs. (5), (6), (7), and (10)] and are only a function of the state of strain in the individual lamina. This type of an approach is particularly useful for displacement formulation analyses, such as closed-form or numerical finite element methods, because it does not require the intermediate calculation of stresses. The stresses are computed only after convergence has been satisfied. The strain in each layer is taken as an average strain for that layer. In general, the strain will not be constant through the ply thickness, but it is an adequate approximation for a relatively thin ply.

Results

Fiber-Dominated Material Nonlinearity Characterization — Test Results

Tow tests (using ASTM D4018[18]) of four different fiber/resin combinations were conducted. These combinations included IM7G/55A, IM7G/DER332, IM7/55A, and AS4/55A. The AS4 and IM7 graphite fibers are two Hercules polyacrylonitrile (PAN) based carbon fibers in which the IM7 has the higher strength and modulus. The IM7G is an IM7 fiber with an epoxy coating. The 55A is the standard Hercules filament winding resin, and the DER332 represents a stoichiometric blend of Dow Chemical's D.E.R. 332, a diglycidyl ether of disphenol A; and Tonox 60/40, a eutectic blend of aromatic daimine curatives and is a common industrial epoxy resin system. For each fiber/resin group, 48 tow specimens were tested. These fiber/resin combinations were analyzed to determine the elastic coefficients (E^o and F).

The four combinations were selected to examine whether the type of resin and sizing had any effect on the measured coefficients. A least-squares curve fit was performed only on specimens that exhibited a smooth stress-strain curve to failure (some specimens exhibited a discontinuous stress-strain curve). The results of the least-squares fit to the tow stress-strain data are summarized in Table 1 for the four systems. The number of specimens analyzed varied from group to group because of the previously mentioned stress-strain curve smoothness consideration. The secant modulus (E_s) that was calculated between 0.1 and 0.6% fiber strain is also listed in the table. It is common practice to report graphite fiber modulus as the secant modulus between 0.1 and 0.6% fiber strain.[11]

It is interesting to note from the table that the measured F and E^o for IM7G/55A, IM7/55A, and IM7G/DER332 are essentially identical. Both size and resin type had no effect on the measured fiber elastic response. This was expected, since it was noted earlier that the resin contribution to the measured stiffness in a tow tensile test is minimal. Another point of interest is that the IM7 and AS4 fiber types exhibit approximately the same degree of nonlinearity, as measured by the magnitude of curvature F. Also listed in Table 1 are data for Amoco high-strength commercial PAN-based graphite fibers, T-700 and T-40.[11] The table indicates that the IM7 elastic coefficients are identical in magnitude to the coefficients measured by Kowalski for the T-40 fiber. These two graphite fibers are advertised as being similar in stiffness and strength characteristics.

Table 1 Elastic coefficients E^o and F test result summary

Fiber/resin type	Number of specimens analyzed	E^o, Msi	F, Msi	E_s,[a] Msi
IM7G/55A	22	38.1	337	40.5
IM7G/DER332	32	38.0	340	40.4
IM7/55A	33	37.6	341	40.0
AS4/55A	23	29.5	347	31.9
T-700[b]	19	35.3	255	37.1
T-40	13	38.7	307	40.8

[a] Calculated between 0.1 and 0.6% strain.
[b] Fiber data for T-700 and T-40 are taken from Ref. 11.

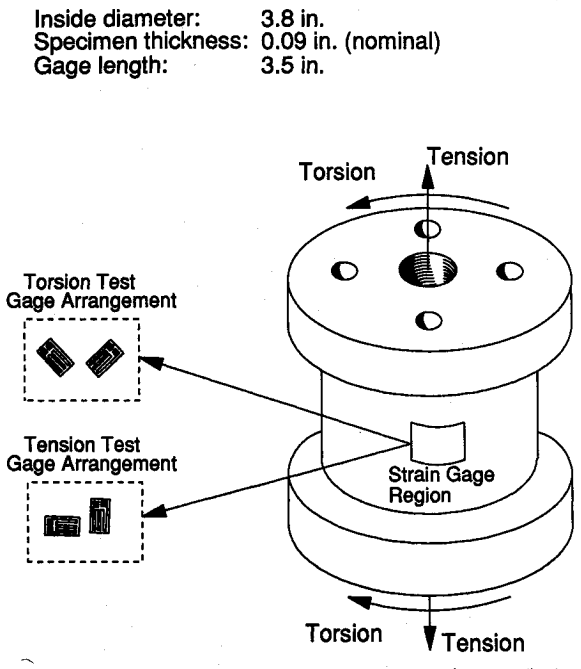

Fig. 2 The 4-in.-diam hoop-wound torsion and transverse tension tubular specimen configuration.

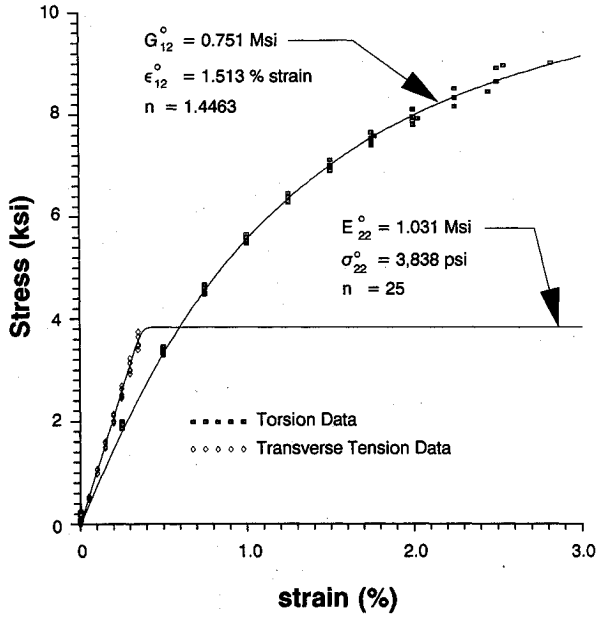

Fig. 3 Lamina matrix-dominated in-plane shear and transverse tension nonlinear stress-strain response for IM7/55A.

Resin-Dominated Material Nonlinearity Characterization—Test Results

The lamina resin-dominated transverse tension and in-plane shear material nonlinearity was characterized with a 4-in. IM7/55A and AS4/55A filament wound tube specimen, which is depicted in Fig. 2. These specimens were loaded both in tension and torsion to failure, and the stress-strain response was recorded electronically. Following the test, the digitized data were fitted with the Richard-Blacklock relationship.

The best least-squares estimate of the parameters in the Richard-Blacklock relation was obtained using a nonlinear regression model that is based on the algorithm developed by Marquardi[19] and is a compromise between using a straight linearization method and a method of steepest descent. The in-plane shear data, together with the best fitted curve, are presented in Figs. 3 and 4 for IM7/55A and AS4/55A, respectively. The goodness of fit of the Richard-Blacklock relation to these data is apparent from both of these figures. The estimates of the parameters are listed in the figure for each of the two fiber/resin combinations. The transverse tension data for the same material systems are also presented. For these data, the lamina initial modulus (E^{o}_{22}) is calculated using a quadratic least-squares fit of the data.

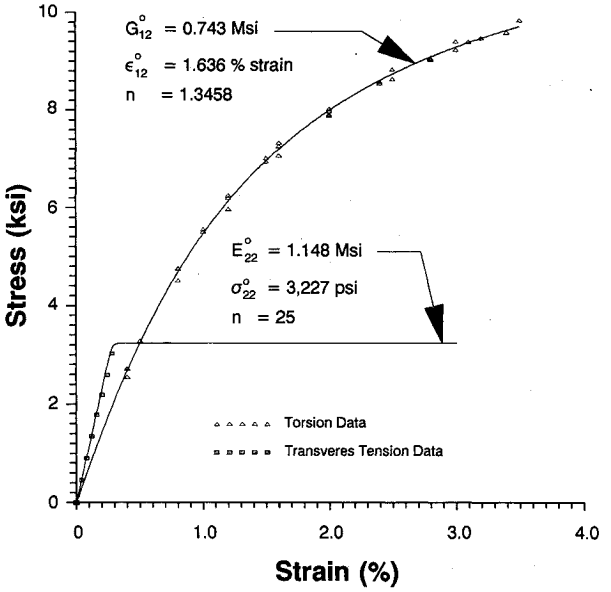

Fig. 4 Lamina matrix-dominated in-plane shear and transverse tension nonlinear stress-strain response for AS4/55A.

The lamina transverse tension strength (σ^{o}_{22}) was taken as the 4-in. tube average transverse tension stress at failure, and n was taken arbitrarily large so that the lamina transverse constitutive relation was idealized as elastic-plastic. Hence, it was assumed that, at the onset of transverse crack, the lamina could no longer carry any load in this direction, which leads to plastic flow. As noted previously, other models have been employed to account for the large reduction in E_{22} following transverse damage. These models range from totally discounting the lamina E_{22} stiffness following damage to a negative tangential modulus, and to a more sophisticated model.[4]

The elastic-plastic model was chosen here because it allows for large degradation in E_{22} following damage, which has physical meaning and is simple to apply within the context of the current analysis. Notice that, given the choice of parameters in the Richard-Blacklock relation to represent E_{22}, the elastic region is essentially linear, which agrees well with the data.

Pressure Vessels Analysis Results

To assess the applicability and improved accuracy in pressure vessel response predictions that result from the inclusion of the aforementioned material nonlinearities in the calculations, two types of 36-in.-diam pressure vessels were analyzed. The first vessel (referred to as vessel A) was fabricated by filament winding of IM7 graphite fiber with 55A winding resin, using the following layup sequence from the cylinder inside diameter to the outside diameter:

$$(\pm 15/90/\pm 15/90/\pm 15/90/\pm 15/90/\pm 15)_t$$

The second vessel (referred to as vessel B) was fabricated by filament winding AS4 graphite fiber and 55A winding resin, using the following layup sequence from the cylinder inside diameter to the outside diameter:

$$(\pm 29/90/\pm 29/90/\pm 29/90/\pm 29/90/\pm 29)_t$$

The asymmetric laminate layup sequence is a typical filament wound pressure vessel construction. The axisymmetric structural applications of these vessel types preclude the out-of-plane coupling response commonly observed in flat panels, except near the cylinder ends. Commonly, in such pressure vessel applications, the straight cylinder section is transitioned smoothly into a dome section and, hence, the effects are minimal. Nevertheless, it is recognized that, in some other applications of such structures, layup sequence interaction with material nonlinearity may be important. The subject of this effect is beyond the scope of this paper. However, it was felt that, in the present investigation, the type of laminate layup sequence should not affect the results and conclusions outcome.

Both vessels consisted of straight cylindrical sections that were approximately 87-in. long. The vessels were pressurized using a specially designed end closure tooling. In the following discussion, the fiber, orientation of ± 15 and ± 29 deg is referred to as helical fiber, and fiber orientation of 90 deg is referred to as hoop fiber. Both fiber orientations are in reference to the cylinder axial direction. A typical range of helical fiber angle orientation for the type of vessels investigated is ± 15–± 30 deg. The angles that were chosen for the analysis were based on the availability of pressure vessel data. During the test, both vessel types were instrumented with numerous axial and hoop foil strain gauges. The A-type vessel was also instrumented with a long wire gauge.

The IM7/55A and AS4/55A principal lamina material properties are shown in Table 2. The values listed for E_{22} and G_{12} are based on the initial moduli, and E_{11} is based on the secant modulus calculated between 0.1 and 0.6% fiber strain and a nominal 0.55 fiber volume fraction. The properties listed are those used in the linear analysis. For a nonlinear analysis, the methodology previously discussed was used while the other lamina properties, except for E_{11}, E_{22}, and G_{12}, were kept constant. Due to the lack of lamina in situ strength properties for the type of material systems studied, σ_{22}^{o} was taken as the transverse failure strength obtained from the 4-in. tube tests (Figs. 3 and 4).

The results of the analysis are presented in Figs. 5–8. Figure 5 is a comparison between the measured and calculated axial and hoop strain response as a function of the internal pressure for the IM7/55A vessel. The test data at hydroproof (approximately 1000 psi) and hydroburst (approximately 1750 psi) are identified by symbols. Data are given for three different vessels. It is apparent from the figure that relatively close predictions were obtained from the two analyses. Because of the fiber strain hardening, the hoop nonlinear pressure-strain curve tends to curve upward with increasing pressure. Fair agreement was obtained between the measured and calculated strains. However, it is also clear that, by rotating the pressure-strain curves clockwise about the origin, perfect agreement can be achieved. This point will be addressed further when the effect of fiber-related parameters, such as fiber volume fraction and fiber orientation on vessel response, is analyzed. The measured strain data presented in Fig. 5 are based on the long wire data, and in general, these data tend to have much less scatter than the foil strain gauge data.

Figure 6 displays similar results to Fig. 5 for the AS4/55A vessel type. The test data in the figure were obtained from foil strain gauges (long wire data were not available). The strain measurement from six vessels indicated much larger scatter was obtained in the hoop strain. It is believed that the hoop strain measurements at hydroburst are inaccurate and, as is apparent from the figure, these data were not available for most vessels, due to gauge failure. These particular vessels were subjected to five proof cycles before burst, which may have contributed to the gauge failure. The axial gauges appear to give accurate readings up to burst. These gauges did not fail, due to the relative low strain in the axial direction. As with the IM7/55A vessel type, the nonlinear and linear analy-

Table 2 Lamina material properties used in the analysis

Property	IM7/55A	AS4/55A
E_{11}, Msi	21.86	17.56
E_{22}, Msi	1.031	1.148
E_{33}, Msi	1.031	1.148
G_{12}, Msi	0.751	0.743
G_{13}, Msi	0.751	0.743
G_{23}, Msi	0.451	0.415
ν_{12}	0.273	0.263
ν_{13}	0.273	0.263
ν_{23}	0.311	0.306
t_{hoop}, in.	0.0292	0.0284
$t_{helical}$, in.	0.0097	0.0123

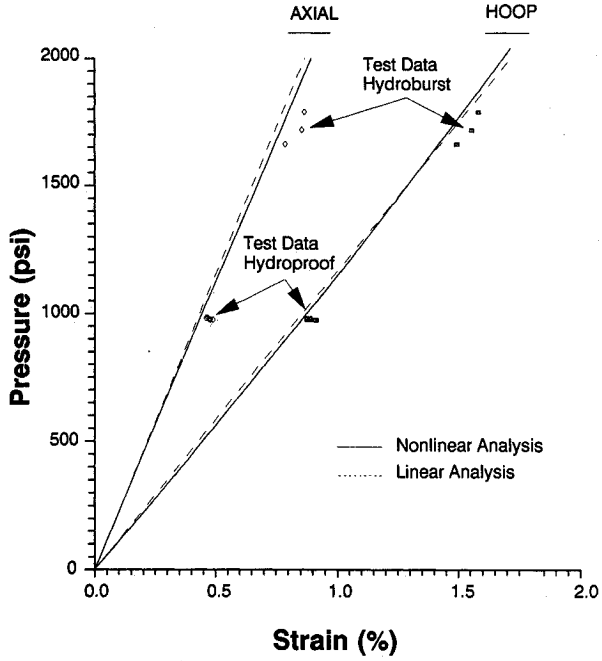

Fig. 5 Comparison between measured and calculated strain response for IM7/55A 36-in. composite pressure vessels.

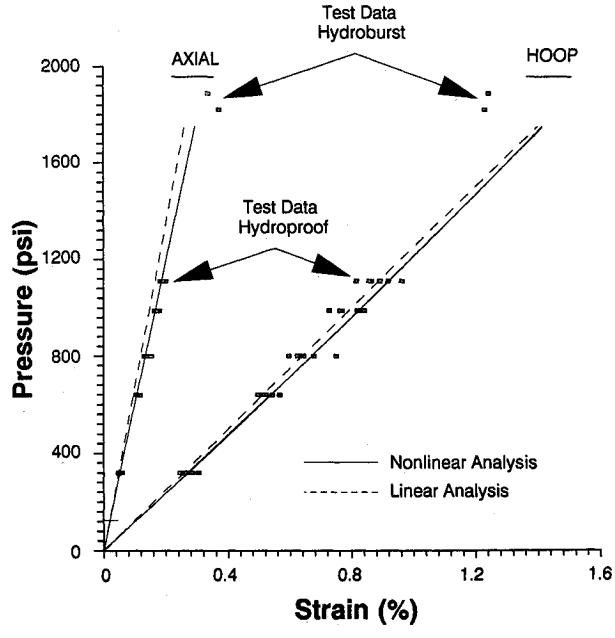

Fig. 6 Comparison between measured and calculated strain response for AS4/55A 36-in. composite pressure vessels.

Table 3 Nonlinear component analysis results (at 1750 psi internal pressure)

Vessel type	Nonlinear analysis type											
	E_{11} only		E_{22} only		G_{12} only		All moduli		Linear analysis		Measured	
	ϵ_H[a]	ϵ_A	ϵ_H	ϵ_A	ϵ_H	ϵ_A	ϵ_H	ϵ_A	ϵ_H	ϵ_A	ϵ_H	ϵ_A
IM7/55A	1.436	0.748	1.506	0.790	1.509	0.745	1.479	0.789	1.508	0.746	1.570	0.851
AS4/55A	1.329	0.290	1.486	0.279	1.422	0.240	1.415	0.294	1.400	0.260	N/A[b]	0.334

[a] ϵ_H = hoop strain, ϵ_A = axial strain in % strain.
[b] Data not available (believed to be inaccurate because of gauge failure).

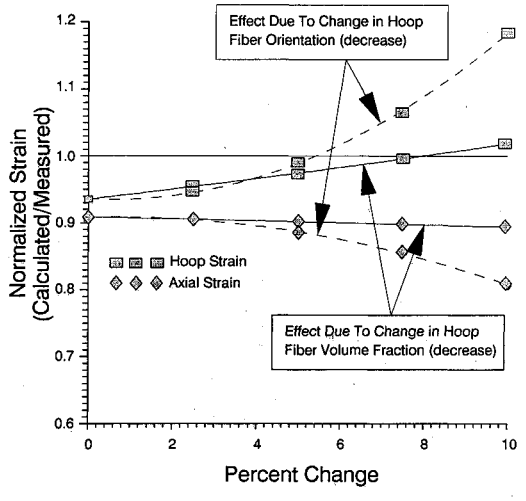

Fig. 7 The effect of variation in hoop fiber orientation and fiber volume fraction on the calculated axial and hoop strain response in the IM7/55A filament wound pressure vessel.

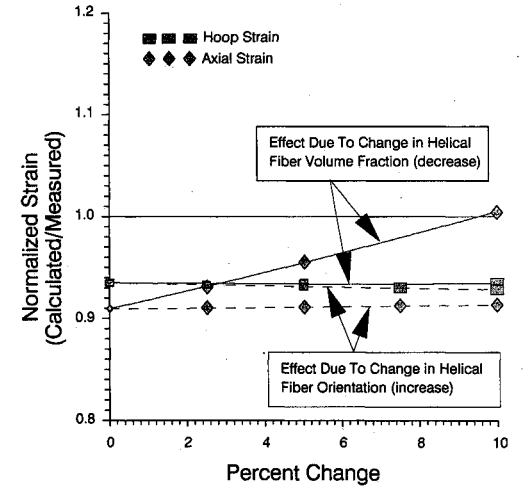

Fig. 8 The effect of variation in helical fiber orientation and fiber volume fraction on the calculated axial and hoop strain response in the IM7/55A filament wound pressure vessel.

ses seem to give similar results, although in the axial direction, the nonlinear analysis seems to produce closer agreement with the measured strain.

To assess the contribution of each material nonlinearity (E_{11}, E_{22}, and G_{12}), each component was considered separately in a nonlinear analysis. The results of this analysis for the IM7/55A and AS4/55A vessels are summarized in Table 3. For comparison, the nonlinear analysis, linear analysis, and actual measured strains are included in the table. The analyses were conducted at 1750 psi internal pressure, which was near the hydroburst pressure for both vessels. The actual measured strain data were interpolated from the actual pressure to 1750 psi.

Before proceeding to discuss the data in Table 3, the reduction in E_{11}, E_{22}, and G_{12} in each layer through the vessel thickness for the IM7/55A and AS4/55A vessel types at 1750 psi internal pressure (summarized in Tables 4 and 5) should be considered. These tables show a large reduction (up to 75%) in E_{22} for the helical layers in both vessels. This is caused by relatively large transverse tension strain on those layers and the elastic-plastic model used to represent the degradation in E_{22} resulting from the anticipated transverse crack damage formation. The reduction in G_{12} is also most noticeable in the helical layers, and is about 14% higher in the AS4/55A vessel type. This is explained by the larger helical fiber orientation in this vessel, which leads to a higher in-plane shear strain deformation and, hence, lower G_{12}. The change in E_{11} is relatively small in all plies. However, because these structures are fiber dominated in their response, particularly in the hoop direction, small changes in E_{11} stiffness may lead to pronounced changes in strain predictions. These changes can be observed from Table 3 by comparing the linear analysis with the nonlinear analysis for E_{11} only.

In general, due to interaction between the three nonlinear components, the individual effect cannot be combined linearly to obtain the overall nonlinear vessel response. However, some response characteristics attributed to each component can be assessed from Table 3. If the data in Tables 3–5 are considered, then the following observations can be made:

1) Lamina fiber nonlinearity, as compared to linear analysis, tends to stiffen the laminate structure response in both the hoop and axial directions and reduce strain in both of these directions, even for a relatively small change in lamina stiffness E_{11}.

2) The lamina E_{22} nonlinearity, as compared to linear analysis, tends to soften the laminate structural response in both the hoop and axial directions and increases strain in both of these directions. However, the change in strains in both directions is relatively small in comparison to the large change in stiffness E_{22}, as noted from Tables 3–5.

3) The lamina G_{12} nonlinearity, as compared to linear analysis, tends to soften the laminate structural response in both the axial and hoop directions. However, the hoop strain tends to increase while the axial strain tends to decrease, due to the 1-to-2 axial-to-hoop pressure vessel force ratio. This effect increases with an increase in the vessel helical fiber angle orientation, as may be observed from comparison between the two vessel types. Nevertheless, a relatively large change in the helical layer in-plane shear stiffness (of up to −25%) produces only a relatively small change in vessel strain response, as compared to the linear analysis (1.6% increase in hoop strain and 7.7% decrease in axial strain).

4) A close look at the contribution of each of the lamina nonlinear components (Table 3) indicates that the linear analysis produces an average result between the stiffening effect of the fiber and the softening effect of the lamina E_{22} and G_{12} nonlinearities.

Overall, the results suggest that all material nonlinearities may be important. However, it is shown that a relatively small change in lamina fiber-dominated nonlinearity produces changes in vessel strain response that are comparable with those produced by relatively large changes in the lamina matrix-dominated material nonlinearities. With the increase in

Table 4 Percent stiffness changes relative to initial stiffness at zero strain in each ply through the IM7/55A vessel thickness (at 1750 psi internal pressure)

Fiber orientation, deg	E_{11}, %	E_{22}, %	G_{12}, %
+15	6.87	−74.30	−8.12
−15	6.96	−74.01	−9.05
90	12.19	−52.76	−0.15
+15	6.96	−74.01	−8.92
−15	6.87	−74.10	−7.99
90	12.14	−52.86	−0.15
+15	6.91	−73.81	−8.92
−15	6.87	−74.01	−7.86
90	12.09	−52.76	−0.15
+15	6.91	−73.81	−8.79
−15	6.87	−73.91	−7.86

Table 5 Percent stiffness changes relative to initial stiffness at zero strain in each ply through the AS4/55A vessel thickness (at 1750 psi internal pressure)

Fiber orientation, deg	E_{11}, %	E_{22}, %	G_{12}, %
+29	6.41	−75.44	−25.30
−29	6.41	−75.35	−25.30
90	16.45	−3.48	−0.05
+29	6.35	−75.26	−25.03
−29	6.41	−75.17	−25.17
90	16.33	−3.48	−0.05
+29	6.35	−75.17	−24.90
−29	6.41	−75.00	−24.90
90	16.20	−3.48	−0.05
+29	6.35	−75.00	−24.76
−29	6.35	−74.91	−24.90

graphite fiber strength (new fibers are targeted to reach a 1 Msi strength), the importance of lamina fiber-dominated nonlinearity will grow even further. Consequently, it is assessed that the lamina fiber-dominated nonlinearity, together with the lamina in-plane shear nonlinearity (for vessels with relatively large helical fiber orientation, say 30 deg and above), can potentially play a significant role in accurate prediction of vessel response for the type of structures discussed. The importance of the lamina E_{22} nonlinearity is somewhat less clear, because this nonlinearity is greatly dependent on the type of damage model incorporated in the analysis. Since the lamina in situ transverse strength is a function of the ply thickness and constraining plies orientations, the large decrease in E_{22} characterized by the elastic-plastic model may overestimate the actual laminate stiffness degradation due to this damage mode. The lack of experimental data precludes making a definitive conclusion regarding the importance of lamina E_{22} nonlinearity. Further, the choice of E_{11}, based on the fiber secant modulus between 0.1 and 0.6% strain, tends to minimize the differences between the linear and nonlinear analyses prediction of axial and hoop strains. If fiber nonlinearity is ignored, the selection of E_{11} based on this approach appears to be preferable to basing it on the initial modulus.

The effect of fiber-related parameters on hoop and axial response is explored further in Figs. 7 and 8, where the two parameters chosen to be varied were the fiber orientation and fiber volume fraction. These particular parameters were chosen based on the degree of uncertainty associated with these parameters in a filament wound structure. Most commonly, the manufacturing tolerance on fiber orientation for a filament wound structure is around ±2 deg, whereas fiber volume fraction can vary 0.50–0.55 and may not be constant through the thickness.

Figure 7 illustrates the effect of variations in hoop fiber orientation and fiber volume fraction on the predicted hoop and axial strains. The analysis was conducted on the IM7/55A vessel type using a nonlinear material model, and the calculated strain was normalized by the measured strain at hydroburst. In Fig. 7, both the helical fiber orientation and fiber volume fraction are decreased by 10% from their nominal 90 deg and 0.55 values. The figure shows that a 10% decrease in the hoop fiber angle to 81 deg resulted in a 25% increase in the predicted hoop strain and an approximately 10.2% decrease in the axial strain, whereas a 10% decrease in the hoop fiber volume fraction to 0.50 leads to an 8.4% increase in the calculated hoop strain and only 1.5% decrease in the axial strain. Figure 8 displays similar results for the effect of variations in the helical fiber orientation and fiber volume fraction on the calculated hoop and axial strains. The results in this figure show that only the fiber volume fraction has a significant effect on the calculated strain. Still, this effect is only pronounced for the axial strain prediction—a 10% decrease in helical fiber volume fraction to 0.50 produced a 10% increase in axial strain. The data presented in Figs. 7 and 8 indicate that the discrepancy noted in Fig. 5 between the calculated and measured strain may be attributed to the degree of uncertainty related to fiber orientation and fiber volume fraction. Ply thickness will also have some effect on these predictions.

Conclusion

A methodology by which fiber and resin-dominated material nonlinearities are incorporated into a composite pressure vessel strain analysis was outlined. Both the composite fiber (E_{11}) and resin (E_{22}, G_{12}) material nonlinearities were evaluated using subscale test specimens. It was shown that fiber nonlinearity in tension can be characterized effectively using fiber tensile tow specimens. The resin-dominated composite nonlinear in-plane shear and transverse tension responses were characterized effectively, using 4-in. filament wound tubes. The fiber material nonlinearity was modeled with a quadratic constitutive relation that is consistent with a third-order polynominal expansion of the strain energy function. The coefficients in this relation were evaluated empirically, using a least-squares best fit to the tow stress-strain data.

The method proposed by Kowalski[11] was used to account for the fiber preload commonly employed in graphite fiber tow tensile test. The lamina E_{22} and G_{12} material nonlinearity was modeled with the Richard-Blacklock relation.[13] The unknown coefficients in this relationship were evaluated empirically, using nonlinear regression techniques and a 4-in. hoop-wound tubular specimen subjected to torsion and transverse tension data. The expected large degradation in E_{22} caused by the formation of transverse cracks was modeled by assuming an elastic-plastic representation of the Richard-Blacklock relation. This was accomplished by setting the parameter n to a relatively large number (i.e., 25) and taking σ_{22}^{o} as the lamina transverse failure strength measured by the 4-in. tube specimens.

Both linear and nonlinear analyses were conducted on two 36-in.-diam cylindrical pressure vessel types. One vessel was fabricated with a filament winding of Hercules IM7 graphite fiber and 55A winding resin and the other by filament winding of Hercules AS4 graphite fiber and 55A winding resin. The results were compared to measured hoop and axial strains on these vessels. The results showed good agreement between the analytical and empirical data, but the linear and nonlinear analyses showed only small differences. A closer look at the contribution of each nonlinear component indicated that the linear analysis produces an average result between the stiffening effect of the fiber and softening effect of the matrix-dominated nonlinearities. It is further shown that a relatively small change in lamina fiber-dominated nonlinearity produces changes in vessel strain response comparable with those produced by relatively large changes in the lamina matrix-dominated material nonlinearities. Therefore, the importance of lamina fiber-dominated nonlinearity will grow even further with the increase in graphite fiber strain to failure. From the results, it is assessed that the lamina fiber-dominated nonlin-

earity, together with the lamina in-plane shear nonlinearity, play the most significant role in accurate prediction of vessel response for the type of structures discussed. The importance of the lamina E_{22} nonlinearity is somewhat less clear, since this nonlinearity is greatly dependent on the type of damage model incorporated in the analysis. Finally, it is shown that the effect of variations in hoop and axial fiber orientations and fiber volume fraction showed that the effects are most pronounced in the hoop fiber.

Acknowledgments

This research was conducted under the Hercules Aerospace Internal Research and Development Program. The author wishes to acknowledge S. H. Cheng, S. C. Ventrello, and B. H. Jenson for providing him with the 4-in. tube data. In addition, the author would like to acknowledge R. W. Bliss for promoting the Richard-Blacklock model.

References

[1]Hahn, H. T., and Tsai, S. W., "Nonlinear Elastic Behavior of Unidirectional Composite Laminate," *Journal of Composite Materials*, Vol. 7, July 1973, pp. 102–108.

[2]Hashin, Z., Bagchi, D., and Rosen, B. W., "Nonlinear Behavior of Fiber Composite Laminates," NASA Rept. CR-2313, 1973.

[3]Sandhu, R. S., "Nonlinear Behavior of Unidirectional and Angle Ply Laminates," *Journal of Aircraft*, Vol. 13, No. 2, Feb. 1976, pp. 104–111.

[4]Nuismer, R. J., and Tan, S. C., "The Role of Matrix Cracking in the Continuum Constitutive Behavior of a Damage Composite Ply," *Mechanics of Composite Materials: Recent Advances*, edited by Z. Hashin and C. T. Herakovich, Pergamon Press, New York, 1982, pp. 437–448.

[5]Petit, P. H., and Waddoups, M. E., "A Method of Predicting the Nonlinear Behavior of Laminated Composites," *Journal of Composite Materials*, Vol. 3, Jan. 1969, pp. 2–19.

[6]Sendeckyj, G. P., Richardson, M. D., and Pappas, J. E., "Fracture Behavior of Thornel 300/5208 Graphite-Epoxy Laminates, Part I: Unnotched Laminates," *Composite Reliability*, ASTM STP 580, 1974, pp. 528–546.

[7]Curtis, J. G., Milne, J. M., and Reynolds, W. N., "Non-Hookean Behavior of Strong Carbon Fibers," *Nature*, Vol. 220, Dec. 1968, pp. 1024–1025.

[8]Ruland, W., "The Relationship Between Preferred Orientation and Young's Modulus of Carbon Fiber," *Applied Polymer Symposia*, No. 9, 1969, pp. 293–301.

[9]Ruland, W., "The Relationship Between Preferred Orientation and Elasticity of Carbon Fibers," *Proceedings of the 9th Carbon Conference*, Boston, MA, 1969, pp. 72–80.

[10]Charles, B. P., Jr., "Strain-Induced Stiffening of Carbon Fibers," *Fiber Science Technology*, Vol. 16, 1982, pp. 219–229.

[11]Kowalski, I. M., "Characterizing the Tensile Stress-Strain Nonlinearity of Polyacrylonitrile-Based Carbon Fibers," *Composite Materials: Testing and Design*, ASTM STP 972, edited by J. D. Whitcomb, 1988, pp. 205–216.

[12]Isikawa, T., Matsushima, M., and Hayashi, Y., "Hardening Nonlinear Behavior in Longitudinal Tension of Unidirectional Carbon Composites," *Journal of Material Science*, Vol. 20, 1985, pp. 4075–4083.

[13]Richard, R. M., and Blacklock, J. R., "Finite Element Analysis of Inelastic Structures," *AIAA Journal*, Vol. 7, No. 3, 1968, pp. 432–438.

[14]Cohen, D., Hyer, M. W., and Tompkins, S. S., "The Effect of Thermal Cycling on Matrix Cracking and Stiffness Changes in Composite Tubes," *Proceedings of the 16th SAMPE Technical Conference*, 1984, pp. 577–588.

[15]Herakovich, C. T., and Hyer, M. W., "Damage-Induced Property Changes in Composites Subjected to Thermal Loading," *Engineering Fracture Mechanics*, Vol. 25, No. 5/6, 1986, pp. 779–791.

[16]Flaggs, D. F., and Kural, M. H., "Experimental Determination of the in Situ Transverse Lamina Strength in Graphite/Epoxy Laminates," *Journal of Composite Materials*, Vol. 16, March 1982, pp. 103–116.

[17]Hyer, M. W., and Rousseau, C. Q., "Thermally-Induced Stresses and Deformations in Angle-Ply Composite Tubes," *Journal of Composite Materials*, Vol. 21, No. 5, May 1987, pp. 454–480.

[18]*ASTM Standards and Literature References for Composite Materials*, 1st ed., ASTM, Philadelphia, PA, 1987.

[19]*Statgraphics, Statistical Graphics System*, STSC Inc., Rockville, MD, 1988.

Earl A. Thornton
Associate Editor